PCCP

PAPER

Cite this: *Phys. Chem. Chem. Phys.*, 2021, **23**, 25720

Received 22nd August 2021,
Accepted 31st October 2021

DOI: 10.1039/d1cp03853b

rsc.li/pccp

Chirality observed in a driven ruthenium-catalyzed Belousov–Zhabotinsky reaction model†

Jason A. C. Gallas [ab]

Chirality is commonly associated with the spatial geometry of the atoms composing molecules, the biochemistry of living organisms, and spin properties. In sharp contrast, here we report chirality found in numerically computed stability diagrams of a chemical reaction governed by purely classical (that is, not quantum) equations, namely in a photochemically periodically perturbed ruthenium-catalyzed Belousov–Zhabotinsky reaction model. This novel chirality offers opportunities to explore hitherto unsuspected properties of purely classical chemical oscillators.

1 Introduction

Asymmetry can be much more eventful than symmetry in disciplines involving chemical and biochemical interactions, as well as optical activity and associated phenomena from the perspective of molecular scattering of polarized light.[1–5] Since the late seventeenth and early eighteen centuries, peculiar optical activity in exquisite crystals and liquids was recognized by Huygens, Haüy, Biot, Fresnel, Pasteur, and others, well before an understanding of the complex three-dimensional nature of molecules. The concept of dissymmetry used in 1848 by Pasteur, aged 25, to describe seemingly identical objects "which differ only as an image in a mirror from the object which produces it" was replaced by the term chirality, introduced much later, in 1893, by Lord Kelvin.[1–3]

Discrepancies between an object and its mirror image, chirality, may be easily recognized in macroscopic objects, like hands and gloves, feet and shoes, scissors, screws, *etc.* However, the most alluring consequences of chirality known today are by far those arising from the quantum realm, associated with the spatial geometry of the atoms composing molecules.

Molecules are ruled by electromagnetic forces, which do not distinguish left from right. Remarkably, with very few exceptions, living organisms use almost exclusively L-amino acids and D-sugars in their biochemistry.[6] Therefore, there seems to be some hidden mechanism enforcing life to be homochiral (to prefer one handedness over the other). Manifestly, it is by no means clear why life on Earth should prefer homochirality, despite ample evidence to this effect.[7–11]

In general, chirality appears mostly in the quantum domain, connected with subtle properties of particle spin, violation of parity operators, and the electroweak interaction.[12] The weak interaction is chiral and thus provides means for exploring chirality in a plethora of enticing situations.[1] The fact that all the aforementioned applications belong to the quantum realm pose a very natural question: is it possible to identify chirality outside the quantum domain, in phenomena governed by purely classical (that is, not quantum) equations?

The aim of this paper is to report the observation of chiral structures, enantiomers, generated by purely classical (that is, not quantum) equations, namely in the complex but regular way that spikes (*i.e.* local maxima) of periodic oscillations organize themselves when control parameters are continuously varied in a model of a photochemically periodically perturbed ruthenium-catalyzed Belousov–Zhabotinsky reaction.[13,14]

Currently, the availability of high-performance computers, combined with efficient and reliable numerical methods, allows computing stability charts summarizing with unprecedented detail the individual behavior of millions of chemical reactions, each one governed by different control parameters.[15–20] As shown below in Fig. 1, 2 and 4, such charts expose remarkable and unanticipated chiral patterns created in phase diagrams by large sets of oscillations with varying waveforms when control parameters are tuned continuously.

It is important to mention at the outset that the chiral patterns reported here are obtained from computer simulations, because they cannot be predicted theoretically due to the total absence of an adequate framework to solve analytically systems of coupled nonlinear differential equations. As described below, chiral patterns emerge as a property of millions of chemical oscillations. Fortunately, however, the

[a] *Instituto de Altos Estudos da Paraíba, Rua Silvino Lopes 419-2502, 58039-190 João Pessoa, Brazil. E-mail: jason.gallas@gmail.com*
[b] *Complexity Sciences Center, 9225 Collins Avenue Suite 1208, Surfside, FL 33154, USA*

† This paper is dedicated to Prof. Richard J. Field, Chemistry Department, University of Montana, on the occasion of his 80th birthday on October 26.

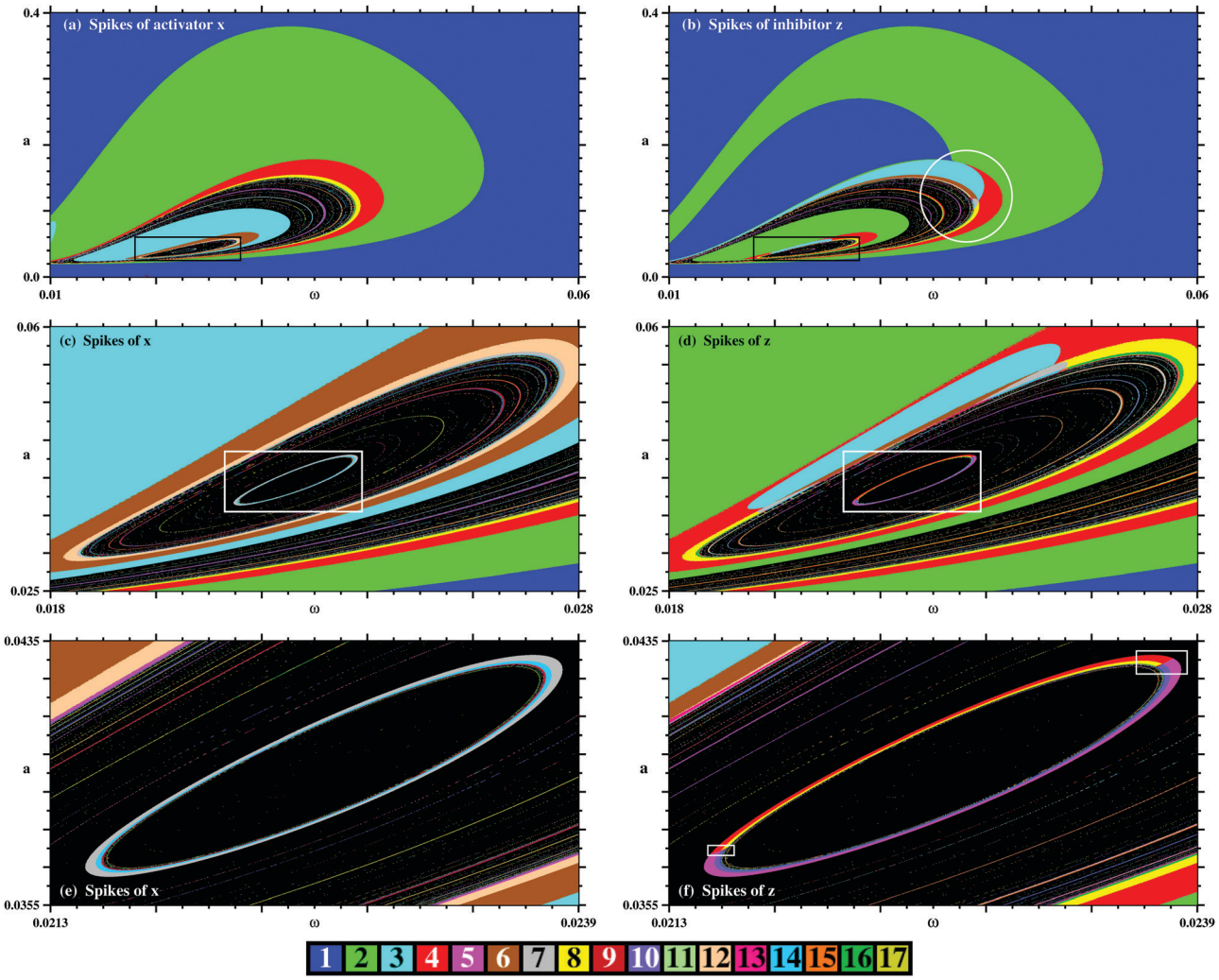

Fig. 1 Frequency-amplitude stability diagrams displaying rings with longitudinally single (left column) or bicolored (right column) paths, obtained by counting spikes per period of the activator x (left column) and the inhibitor z (right column) of the driven Belousov–Zhabotinsky reaction. Top row: Main views of the control space. The circle in panel (b) highlights the region containing the quint points discussed in ref. 13. Center row: (c) and (d) Show magnifications of the black boxes in (a) and (b), respectively. Bottom row: (e) and (f) show magnifications of the boxes in (c) and (d), respectively, showing sequences of concentric rings extending as far as the eye can see. Colors represent the number of spikes per period as indicated by the common colorbar at the bottom. Black denotes parameters leading to non-periodic (chaotic) oscillations. In panel (f), the pair of white boxes indicates where color-mediating chiral transitions are located. These boxes are shown magnified in Fig. 2. Each panel of this figure displays the analysis of individual oscillations for grids with $1200 \times 1200 = 1.44 \times 10^6$ equally spaced parameter points.

chirality of the Belousov–Zhabotinsky reaction may be validated experimentally, as described in the last paragraph of Section 4.

2 Ruthenium-catalized BZ reaction

The Belousov–Zhabotinsky (BZ) reaction has a rich and distinguished history.[21–23] It is the prototype of a chemical reaction governed by a nonlinear dynamic law and exhibiting oscillations in the concentrations of intermediate species. In the classic BZ reaction the driving chemical reaction is the oxidation of malonic acid ($CH_2(COOH)_2$) by bromate ion (BrO_3^-) in aqueous 1 M H_2SO_4. The direct reaction between BrO_3^- and malonic acid is very slow, and it is typically catalyzed by a redox couple consisting of two metal ions separated by a single electron, *e.g.*, Ce(III)/Ce(IV) in the classic recipe, or by similar couples, *e.g.*, $Fe(phen)_3^{2+}/Fe(phen)_3^{3+}$ and $Ru(phen)_3^{2+}/Ru(phen)_3^{3+}$ with phen ≡ phenanthroline. The Ru-catalyzed system[24–26] is interesting because it can be perturbed *via* light absorption by $Ru(phen)_3^{2+}$ to yield the excited species $Ru^*(phen)_3^{2+}$, which eventually leads to generation of Br^-, the species that controls the BZ oscillations. This photochemically perturbed system is the object of our investigation.

Field, Körös and Noyes (FKN)[27] described in 1972 the BZ chemical mechanism as consisting of nine reactions involving eight intermediates.[13] This mechanism has very largely stood the test of time.[21,28] Field and Noyes[29] used rate-determining step approximations to reduce the FKN mechanism to a system

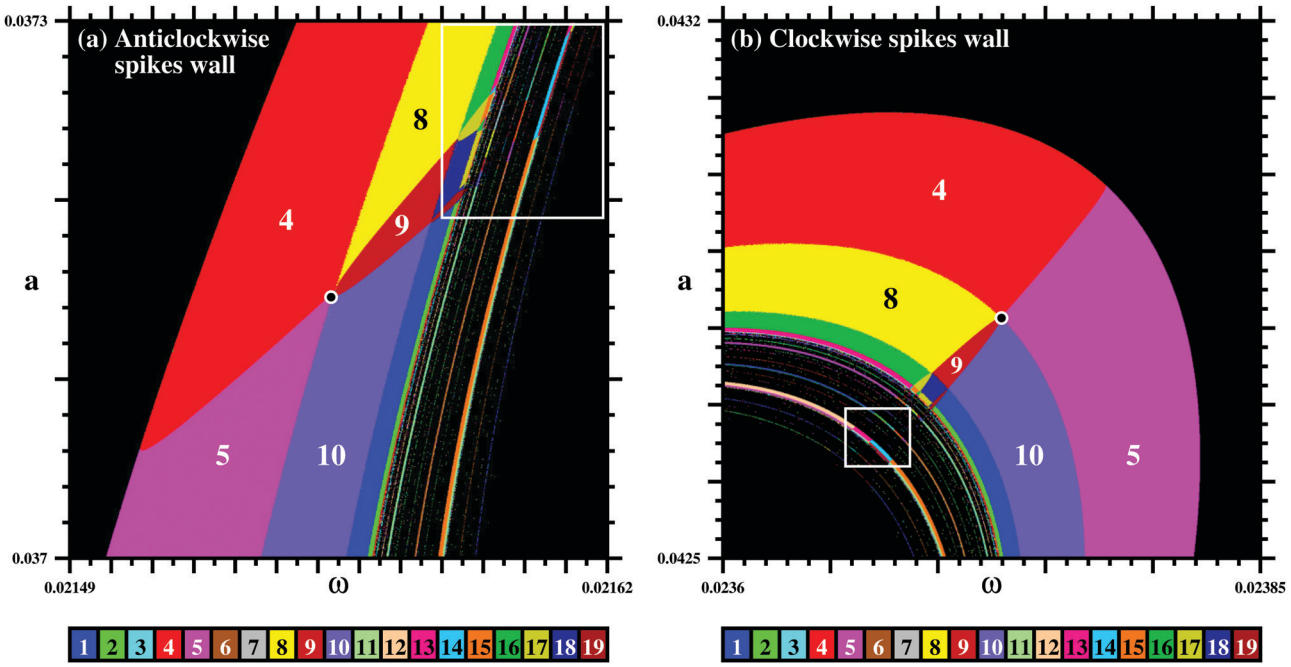

Fig. 2 Magnifications of the two possible enantiomers (mirror-images of the adding-doubling spikes walls) that guarantee the correct continuity of the phases needed to form rings, *i.e.* closed loops, in the control plane of the inhibitor z seen in Fig. 1(f). Numbers refer to the number of spikes per period of the individual phases. (a) A-cascade: the number of spikes grows anticlockwise. (b) C-cascade: the number of spikes grows clockwise. Black dots mark the first quint point[13] of a lattice of boundary points where five distinct stability phases with different number of spikes meet. White boxes show that color changes spill over well into the phase of chaos. The box in panel (b) is magnified in Fig. 4. Panels show the analysis of 1200 × 1200 = 1.44 × 10^6 equally spaced parameter points.

of three variables: [$HBrO_2$], [Br^-] and [Ce(IV)], that together define the dynamic structure of the BZ reaction. The scaled kinetic equations form the so-called Oregonator model, namely

$$\begin{aligned} \varepsilon\frac{dx}{dt} &= x(1-x) + y(q-x), \\ \sigma\frac{dy}{dt} &= \eta z - y(q+x), \\ \frac{dz}{dt} &= x - z. \end{aligned} \tag{1}$$

The dimensionless parameters ε, σ and q contain information about the rate equations of the five irreversible steps of the reduced mechanism and the concentrations of malonic acid. Typical values are $\sigma \ll \varepsilon$, $q \ll 1$. The time scales of x and y are similar and both much faster than z. Thus it is possible to reduce eqn (1) to two variables either by causing x to follow y (set $dx/dt = 0$) or by causing y to follow x (set $dy/dt = 0$). Tyson[30] and Tyson and Fife[31] showed that y is a little faster than x (and the result less complex) and set $dy/dt = 0$ obtaining thereby $y = \eta z/(q + x)$. The photosensitivity of the Ru-catalyzed BZ reaction allows an opportunity to investigate its behavior under external, periodic, light-perturbation $I(t)$ that is simply added to the activator (autocatalytic, here x) equation with little regard to the actual chemistry occurring. Therefore, after simple rescaling $z \leftarrow \eta z$ and $t \leftarrow t/\varepsilon$ the model becomes,[13,14]

$$\frac{dx}{dt} = \frac{1}{10}\left[x(1-x) + \frac{q-x}{q+x}z + I(t)\right], \tag{2}$$

$$\frac{dz}{dt} = \frac{\varepsilon}{10}(\eta x - z), \tag{3}$$

where $I(t) = a\sin(\omega t)$ is an external periodic perturbation with frequency ω and amplitude a. Following the literature,[13,14] we fix $q = 0.1$, $\varepsilon = 0.025$, and $\eta = 5$, and investigate the dynamics as a function of ω and a.

3 Computational details

To characterize the stability of the distinct oscillatory phases of the BZ reaction, we compute the so-called isospike diagrams.[15,16,20] Briefly, we select $\omega \times a$ windows of interest and cover them with discrete grids containing $N \times N$ equidistant points. For each point of such grids, the temporal evolution of the reaction is determined numerically by solving eqn (2) and (3) similarly as done in ref. 13, namely using the standard fourth-order Runge–Kutta algorithm with a fixed time-step 0.002, starting from the arbitrary initial condition $(x, z) = (0.16, 1.6)$ and following the attractor[16,20] horizontally from left to right.

For each point (ω, a) on the grid we determined whether or not the spikes (local maxima) of x and z repeated, recording with suitable colors the number of spikes per period for periodic oscillations, and with black those oscillations found to be nonperiodic (chaotic). In this simple and computationally efficient way one obtains the the so-called isospike

diagrams,[15–17,20] depicting parameter domains characterized by oscillations which share a common number of spikes. Such diagrams reproduce the content of standard Lyapunov classification but with a significant advantage: instead of lumping together all periodic oscillations into just a single large phase as Lyapunov diagrams do, isospike diagrams display directly the number of spikes of the individual oscillations for every grid point $\omega \times a$. Therefore, isospike diagrams allow one to immediately visualize how the number of spikes evolves as a function of the frequency ω and amplitude a of the external drive.

By selecting sufficiently fine grids of points, the discrete stability diagrams look visually continuous. Here we use grids displaying the analysis of reactions over $\omega \times a$ parameter sets containing $1200 \times 1200 = 1.44 \times 10^6$ equidistant points. The panels composing Fig. 1 and 2 are examples of some of the isospike diagrams obtained. Clearly, the quality of the final diagrams, as well as the computational work needed to obtain them, depends sensitively on the number of points used for the grids. High resolution diagrams are usually computationally very demanding to obtain. For detailed surveys on the computation of stability diagrams see ref. 15 and16.

4 Chiral rings

Fig. 1 shows stability diagrams displaying successive magnifications computed for the driven Belousov–Zhabotinsky reaction of eqn (2) and (3). The left column shows diagrams obtained by counting spikes per period of the activator x, while the right column shows the corresponding diagrams for the inhibitor z. Colors are used to represent phases characterized by periodic oscillations while black marks parameters for which non-periodic (chaotic) oscillations are found.

Similarly to familiar differences observed when attractors are projected in distinct phase-space planes, the stability diagrams of Fig. 1 display different aspects of the multidimensional control space when inspected by counting spikes with distinct variables of the system. However, although the number of spikes per period may differ for distinct variables, the oscillation period measured is always the same, as it should be, independently of the variable used to determine it. Manifestly, pairs of stability diagrams in Fig. 1 have distinct boundaries among phases of periodic oscillations. Although the shape and extension of the global periodic phases clearly agree for both variables, the number of spikes of individual phases is seen to depend significantly on the variable used to determine them. As already mentioned, this is the important feature of isospike diagrams.

The pair of diagrams on the top row of Fig. 1 show extended windows of the control space. The region inside the circle in panel (b) displays a lattice of quint points,[13] namely points where five stable phases of oscillation with different numbers of spikes per period meet. The windows of interest here are indicated by the black boxes in Fig. 1(a) and (b). Such boxes are magnified in Fig. 1(c) and (d). In these panels it is possible to identify a series of concentric ovals, closed parameter circuits, some of them rather thin in the scale of these figures. The white box at the center of panels 1(c) and 1(d) contains ticker rings, magnified in Fig. 1(e) and 1(f). Longitudinally, the adjacent rings in panel 1(e) display just a single color, thereby characterizing periodic oscillations with the same number of spikes per period along the whole circuits. In sharp contrast, the circuits in panel 1(f) display two colors, indicating that the number of spikes changes when circulating along them. These color changes occur for the thiner rings seen in both Fig. 1(e) and 1(f): along the circuits, colors may either change, as in panel (f), or not, as in panel (e). Of interest here are color changes which occur longintudinally along rings of periodic oscillations, like in Fig. 1(d) and 1(f).

Fig. 2 shows in greater detail how colors (*i.e.* the number of spikes per period) change longitudinally inside the pair of small white boxes seen in Fig. 1(f). It is natural to think that colors could have changed in a simple way, as it occurs transversally in Fig. 1(e). And, as may be seen in both panels of Fig. 2, this is what indeed happens between the phases changing from 4 to 5 spikes per period. However, in the next level $8 \to 9 \to 10$, colors change longitudinally in a rather exquisite and intricate way. In the next level, namely $16 \to 17 \to 18 \to 19 \to 20$, the number of spikes per period changes in an analogous way, revealing a regular pattern. This regular growth of the number of spikes repeats in the next levels, although it becomes more and more difficult to identify such changes on the scale of these panels. Thus, one sees that the most prominent color stripes of the ''external'' spikes-doubling cascades 4×2^n and 5×2^n visible in Fig. 1(f) are mediated by complex but regular adding-doubling spikes structures which, for simplicity, we refer to as ''walls'' of spikes. These very localized color walls mediate color changes along rings and filaments in control space.

A cursory comparison of the walls seen in Fig. 2(a) and (b) may give the impression that their spikes unfolding coincide, but this is not the case. These walls are very distinct from each other, forming a regular and artfully asymmetric chiral pair, each one involving identical combinations of adding and doubling cascades of spikes but arranged in a distinct order. To see this, compare the phases $u = 4$ and $v = 5$ where the transversal cascades $u \times 2^n$ and $v \times 2^n$ forming the bicolored outer rings start in Fig. 1(f). While in Fig. 2(a) the number of spikes increase anticlockwise, in Fig. 2(b) they clearly increase clockwise. The same happens for the next level of stripes, namely $8 \to 9 \to 10$, and so on.

Fig. 3 summarizes schematically the first few levels of spikes unfolding present in Fig. 2. Manifestly, from Fig. 3 it is not difficult to realize that the two walls turn out to be chiral images when reflected on the schematic mirror that separates them. A remarkable feature of the chiral structures generated by the Belousov–Zhabotinsky reaction is that they arise from a self-organization of many oscillations of the reaction, not from a property of any isolated oscillation. To see them, one needs to tune two independent control parameters of the reaction.

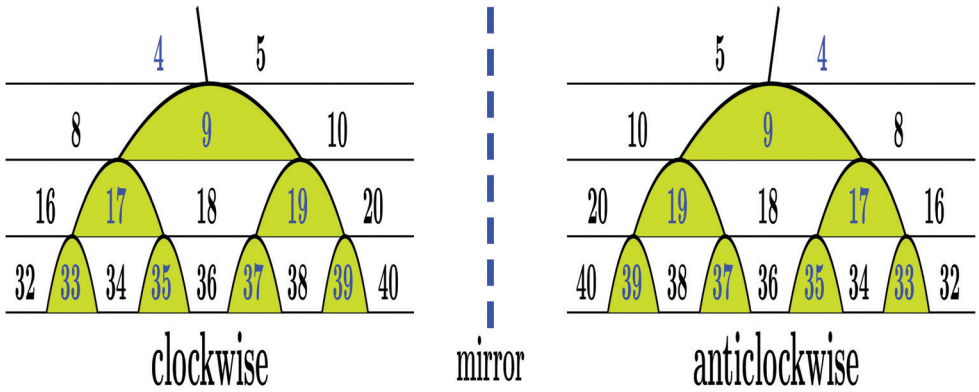

Fig. 3 Schematic representations of the two types of chiral walls that bridge ring segments characterized by different numbers of spikes, indicated by the numbers. When moving along a ring, like in Fig. 1(f), the number of spikes may increase either clockwise or anticlockwise. The number of spikes of the parabolic-like arcs is always odd, given by the sum of the two phases with the smallest number of spikes that meet at quint points,[13] vertex of the parabolas. For instance, 9 = 4 + 5, 17 = 8 + 9, *etc.* The chiral walls involve simultaneous combinations of adding and doubling spikes cascades[19].

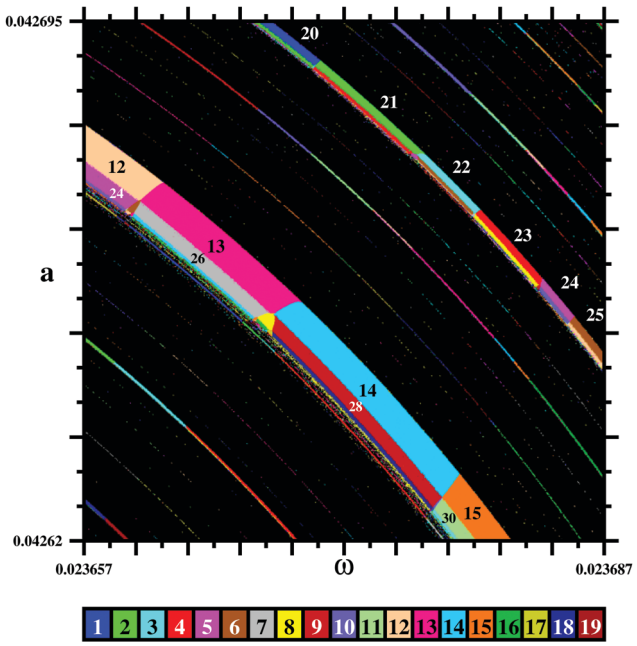

Fig. 4 Magnification of the white box seen in Fig. 2(b) showing that the clockwise oriented walls of inhibitor z-spikes spillover into the stripes of periodic oscillations embedded in the black phase of chaos, causing them to be multicolored, namelyreflecting their varying number of spikes. Numbers refer to the number of spikes per period of z. The number of walls increase as stripes get thiner and thiner and the number of spikes simultaneously increases. A similar spillover occurs for anticlockwise oriented walls as seen, *e.g.*, in the white box in Fig. 2(a). Resolution: $1200 \times 1200 = 1.44 \times 10^6$ equally spaced parameter points.

Fig. 4 shows that the color changes are not restricted to the initial cascading of periodic oscillations of the BZ reaction, but that extend well into the periodic phases interspersed inside the phases of chaos, or sandwiched with them. Furthermore, Fig. 4 also show that, mutatis mutandis, the cascading illustrated in Fig. 3 is also present in all the smaller and smaller periodic phases, windows, embedded in chaos.

How could one experimentally measure chiral structures in the driven Belousov-Zhabotinsky reaction? One possibility is to record experimental stability diagrams analogous to the ones in Fig. 1, 2, and 4. An analogous experimental recording was done before for an electronic circuit.[32] However, this procedure is anticipated to be a challenging task due mainly to the necessity of maintaining the reaction constant over long periods of time and, simultaneously, having the ability to discriminate small spikes differences. Fortunately, a much simpler way to measure BZ chirality is suggested by the sequences of numbers which represent the spikes distributions in Fig. 2 and 4. Since one now knows what to expect from the spikes distributions, it is enough to just record and compare the temporal evolution of the spikes of the inhibitor z for parameter points located inside adjacent windows like, for instance, $4 \rightarrow 5$, or $8 \rightarrow 9 \rightarrow 10$ or even in the longer and more elusive chaos embedded series $12 \rightarrow 13 \rightarrow 14 \rightarrow 15$ seen in Fig. 4, and similar ones. Comparing such simple temporal signals can identify unambiguously BZ chirality.

5 Conclusions and outlook

As schematically summarized in Fig. 3, this paper reports the observation of adding-doubling chiral walls of spikes in the frequency *versus* amplitude parameter plane of a driven Belousov–Zhabotinsky reaction described by eqn (2) and (3). Spikes walls are found along certain closed parameter loops. They mediate families of stable oscillations with different number of spikes (local maxima) per period. Chiral walls are seen while recording how the number of spikes of the oscillations evolve when the control parameters of the purely classical equations are varied. In other words, this chirality is not related to standard chiralities of quantum origin.

The chiral structures reported here can be observed only through either computer simulations or experimental work. The reason for this is that chirality is difficult, not to say impossible, to establish theoretically due to the total absence of any adequate framework to obtain analytical solutions for

systems of nonlinearly coupled differential equations over arbitrary parameter ranges. Fortunately, as described, the chirality of the BZ reaction is clearly accessible to experimental validation.

From an applied point of view, the existence of chirality in the BZ reaction is a most surprising phenomenon. This chirality revises current knowledge about the intricate topology of the control space of a BZ reaction, a prototypic model of a chemical oscillator, and offers opportunities to investigate hitherto unsuspected properties and the whys and wherefores of analogous reactions governed by classical (that is, not quantum) equations. For instance, the unfolding of the dual wall pairs in Fig. 2 and 3 is found to depend exclusively on the relative magnitude of the integers $u = 4$ and $v = 5$ where the walls start. A challenging question is to understand the underlying dynamical mechanisms leading to the formation of the walls and the selection of either $u < v$ or $u > v$, as well as to the observed order A, C or C, A of the walls spread along rings and filaments.

Finally, we briefly mention that we observed chirality very recently in another rather distinct system governed by classical equations, namely in Hartley's electronic circuit[33], involving a rather distinct and autonomous (*i.e.* time independent) system. Further promising systems with classical equations and likely to display classical chirality are systems displaying rings[34] and the so-called ''eyes of chaos'', *e.g.*, in the periodically driven Brusselator,[35] in a rotor system with oil-film force,[36] in an electronic circuit based on the startling memristor element,[37] and possibly in other applications.[38,39] Consequently, we expect chirality generated by classical equations to be a generic property of a wide class of systems and to underly interesting novel applications that remain to be discovered.

Conflicts of interest

There are not conflicts of interest to declare.

Acknowledgements

This work was started during a visit to the Max-Planck Institute for the Physics of Complex Systems, Dresden, gratefully supported by an Advanced Study Group on Forecasting with Lyapunov vectors. The author was partially supported by CNPq, Brazil, grant PQ-305305/2020-4. All bitmaps were computed at the CESUP-UFRGS Supercomputer Center of the Federal University in Porto Alegre, Brazil.

References

1 G. H. Wagnière, *On Chirality and the Universal Asymmetry: Reflections on Image and Mirror Image*, Wiley-VCH, Weinheim, 2007.
2 L. Barron, *Molecular Light Scattering and Optical Activity*, Cambridge University Press, Cambridge, 2nd edn, 2004.
3 G. B. Kauffman and R. D. Myers, Pasteur's resolution of racemic acid: A sesquicentennial retrospect and a new translation, *Chem. Educ.*, 1998, **3**, 1–18, DOI: 10.1333/s00897980257a.
4 W. Ma, L. Xu, A. F. de Moura, X. Wu, H. Kuang, C. Xu and N. A. Kotov, Chiral inorganic nanostructures, *Chem. Rev.*, 2017, **117**, 8041–8093.
5 E. Sanganyado, Z. Lu, Q. Fu, D. Schenk and J. Gan, Chiral pharmaceuticals: A review on their environmental occurrence and fate processes, *Water Res.*, 2017, **124**, 527–542.
6 L. G. Wade Jr. and J. W. Simek, *Organic Chemistry*, 9th edn, Pearson, Harlow, 2017.
7 R. A. Hegstrom, β decay and the origins of biological chirality: theoretical results, *Nature*, 1982, **297**, 643–647.
8 R. A. Hegstrom and D. K. Kondepudi, The handedness of the Universe, *Sci. Am.*, 1990, **262**(1), 108–115.
9 R. A. Rosenberg, M. Abu Hija and P. J. Ryan, Chiral-selective chemistry induced by spin-polarized secondary electrons from a magnetic substrate, *Phys. Rev. Lett.*, 2008, **101**, 178301.
10 P. de Marcellus, *et al.*, Non-racemic amino acid production by ultraviolet irradiation of achiral interstellar ice analogs with circularly polarized light, *Appl. J. Lett.*, 2011, **272**, L27.
11 J. M. Dreiling and T. J. Gay, Chirally sensitive electron-induced molecular breakup and the Vester-Ulbricht hypothesis, *Phys. Rev. Lett.*, 2014, **113**, 118103.
12 S. Weinberg, Conceptual foundations of the unified theory of weak and electroweak interactions, *Rev. Mod. Phys.*, 1980, **52**, 515–523.
13 R. J. Field, J. G. Freire and J. A. C. Gallas, Quint points lattice in a driven Belousov-Zhabotinsky reaction model, *Chaos*, 2021, **31**, 053124.
14 M. I. Español and H. G. Rotstein, Complex mixed-mode oscillatory patterns in a periodically forced excitable Belousov-Zhabotinsky reaction model, *Chaos*, 2015, **25**, 064612.
15 J. G. Freire and J. A. C. Gallas, Stern-Brocot trees in the periodicity of mixed-mode oscillations, *Phys. Chem. Chem. Phys.*, 2011, **13**, 12191–12198.
16 J. A. C. Gallas, Spiking systematics in some CO_2 laser models, Invited review paper, *Adv. At., Mol., Opt. Phys.*, 2016, **65**, 127–191.
17 C. S. Rodrigues, C. G. P. dos Santos, C. C. de Miranda, E. Parma, H. Varela and R. Nagao, A numerical investigation of the effect of external resistence and applied potential on the distribution of periodicity and chaos in the anodic dissolution of nickel, *Phys. Chem. Chem. Phys.*, 2020, **22**, 21823–21834.
18 J. A. C. Gallas, Lasers, stability, and numbers, *Phys. Scr.*, 2019, **94**, 014003.
19 J. A. C. Gallas, Overlapping adding-doubling spikes cascades in a semiconductor laser proxy, Brazilian, *J. Phys.*, 2021, **51**, 919–926.
20 J. A. C. Gallas, M. J. B. Hauser and L. F. Olsen, Complexity of a peroxidase-oxidase reaction model, 2021 PCCP HOT Article, *Phys. Chem. Chem. Phys.*, 2021, **23**, 1943–1955.

21 A. M. Zhabotinsky, *Scholarpedia*, 2007, **2**(9), 1435, DOI: 10.4249/Scholarpedia.1435.
22 *Chaos in Chemistry and Biochemistry*, ed. R. J. Field and L. Györgyi, World Scientific, Singapore, 1993.
23 For a survey see: R. J. Field, Chaos in the Belousov-Zhabotinsky reaction, *Mod. Phys. Lett. B*, 2015, **29**, 1530015.
24 R. Toth and A. Taylor, The tris(2,2′-Bipyridyl) ruthenium-catalyzed Belousov-Zhabotinsky reaction, *Prog. React. Kinet. Mech.*, 2006, **31**, 59–115.
25 S. Kitawaki, K. Shiori, T. Sakurai and H. Kitahata, Control of the self-motion of a ruthenium-catalyzed Belousov-Zhabotinsky droplet, *J. Phys. Chem.*, 2012, **116**, 26805–26809.
26 K. P. Zeyer and F. W. Schneider, Periodicity and chaos in chemiluminescence: The ruthenium-catalyzed Belousov–Zhabotinsky reaction, *J. Phys. Chem. A*, 1998, **102**, 9702–9709.
27 R. J. Field, E. Körös and R. M. Noyes, Oscillations in chemical systems II. Thorough analysis of temporal oscillation in the bromate-cerium-malonic acid system, *J. Am. Chem. Soc.*, 1972, **94**, 8649–8664.
28 A. F. Taylor, The Belousov-Zhabotinsky reaction, *Prog. React. Kinet. Mech.*, 2002, **27**, 247–325.
29 R. J. Field and R. M. Noyes, Oscillations in chemical systems IV. Limit cycle behavior in a model of a real chemical reaction, *J. Chem. Phys.*, 1974, **60**, 1877–1884.
30 J. J. Tyson, A Quantitative Account of Oscillations, Bistability, and Traveling Waves in the Belousov–Zhabotinsky Reaction, in *Oscillations and Traveling Waves in Chemical Systems*, ed. R. J. Field and M. Burger, Wiley-Interscience, New York, 1985.
31 J. J. Tyson and P. C. Fife, Target patterns in a realistic model of the Belousov-Zhabotinsky reaction, *J. Chem. Phys.*, 1980, **73**, 2224–2237.
32 A. Sack, J. G. Freire, E. Lindberg, T. Pöschel and J. A. C. Gallas, Discontinuous spirals of stable periodic oscillations, *Sci. Rep.*, 2013, **3**, 3350.
33 J. A. C. Gallas, Chirality detected in Hartley's electronic oscillator, *Eur. Phys. J. Plus*, 2021, **136**, 1048.
34 G. M. Ram rez-Ávila, J. Kurths and J. A. C. Gallas, Ubiquity of ring structures in the control space of complex oscillators, *Chaos*, 2021, **31**, 101102.
35 J. A. C. Gallas, Periodic oscillations of the forced Brusselator, *Mod. Phys. Lett. B*, 2015, **29**, 1530018.
36 X. B. Rao, Y. D. Chu, Y. X. Chang, J. G. Zhang and Y. P. Tian, Dynamics of a cracked rotor system with oil-film force in parameter space, *Nonlinear Dyn.*, 2017, **88**, 2347–2357.
37 X. B. Rao, X. P. Zhao, J. S. Gao and J. G. Zhang, Self-organizations with fast-slow time scale in a memristor-based Shinriki's circuit, *Commun. Nonlin. Sci. Numer. Simul.*, 2021, **94**, 105569.
38 J. H. E. Cartwright, J. M. Garc a-Ruiz, O. Piro, C. I. Sainz-Daz and I. Tuval, Chiral symmetry breaking during crystallization: an advection-mediated nonlinear autocatalytic process, *Phys. Rev. Lett.*, 2004, **93**, 035502.
39 B. Li, L. Deng and H. Zhang, Chiral symmetry breaking in a reaction-diffusion system, *Phys. Rev. E: Stat., Nonlinear, Soft Matter Phys.*, 2013, **87**, 042905.

